


Bacteria-Assisted Celastrol Liposomes for Effective Chemotherapy Against Lung Cancer in Mice Model

Xinyi Wang, Chao Gao, Xialin Zhang, Yingqi Gu, Shaozhi Fu , Sheng Lin

Department of Oncology, the Affiliated Hospital of Southwest Medical University, Luzhou, 646000, People's Republic of China

Correspondence: Shaozhi Fu; Sheng Lin, Email shaozhifu513@swmu.edu.cn; lslinsheng@163.com

Introduction: Lung cancer has a high resistance rate to current chemotherapies. Therefore, there is an urgent need to develop new anticancer drugs. Celastrol is a promising anticancer bioactive compound for various types of cancers. However, its poor solubility and severe liver damage have limited its clinical application.

Methods: BIF@CEL/LF/CMCS-Lipo (Bif@CLC-LP), a self-driving biomotor that targets tumor tissues, was used to deliver celastrol, which was encapsulated in surface-modified lactoferrin liposomes, which were then coated with carboxymethyl chitosan and loaded onto the surface of *Bifidobacterium infantis* (Bif). Extensive in vitro and in vivo experiments were performed to assess its physicochemical and antitumor properties and safety in treating lung cancer.

Results: Bif@CLC-LP responds to pH and is bioselective, precisely targeting hypoxic regions of tumors. In the acidic tumor environment, the carboxymethyl chitosan coating breaks down, releasing liposomes that can specifically target the cancer surface receptor for endocytosis. This process increases the production of reactive oxygen species (ROS) and decreases the mitochondrial membrane potential in lung cancer cells, leading to apoptosis.

Conclusion: In our work, Bif@CLC-LP significantly inhibited tumor growth while minimizing celastrol-induced liver damage in a mouse lung cancer model. This bacteria-mediated liposome delivery system is a promising new nanoplatform for treating different types of solid cancer.

Keywords: *bifidobacterium infantis*, celastrol, liposome, lactoferrin, chemotherapy

Introduction

Lung cancer is the most common type of cancer worldwide and the leading cause of cancer-related death.¹ Chemotherapy remains an essential part of systemic therapy for treating lung cancer, even though neoadjuvant treatments such as immunotherapy and targeted medications have been developed.^{2,3} However, challenges such as drug resistance, poor drug bioavailability, inadequate targeting, and significant systemic toxicity often hinder the effectiveness of chemotherapy in treating lung cancer.⁴ Therefore, chemotherapeutic drugs with greater efficacy and lower toxicity need to be developed.⁵

Celastrol is a quinone methoxy triterpenoid molecule derived from the root bark of the plant *tretinoin*.⁶ Its pharmacological properties, including its ability to inhibit tumor growth, reduce inflammation, and facilitate weight reduction, have been extensively investigated.⁷ Studies have confirmed that cancer cells treated with celastrol exhibit significantly high levels of ROS and mitochondrial damage, leading to apoptosis.^{8,9} Celastrol strongly inhibits the growth of various types of human cancer cells and has shown strong anticancer effects in various mouse models of tumors, including lung cancer,¹⁰ hepatocellular carcinoma,¹¹ glioma,¹² and melanoma.¹³

Liposomes are widely used as carriers for delivering anticancer drugs to improve their efficacy and reduce systemic toxicity.¹⁴ Therefore, the biocompatibility, lack of immunogenicity, degradability, and other advantages of liposomes make them excellent clinical drug carriers.¹⁵ PEGylated liposomes form a hydration layer on their surface, decreasing their absorption by regular tissues and preventing the reticuloendothelial system from ingesting the drug, thus increasing drug levels in the bloodstream and improving the effectiveness of the drugs.¹⁶

Additionally, the surface expression of the lactoferrin receptor and its metabolic activity are high in cancer cells.¹⁷ This property can be used to create a targeted delivery system that significantly increases the potency of anticancer drugs.¹⁸ Lactoferrin is a naturally occurring protein with antibacterial and anticancer properties.¹⁹ When lactoferrin is attached to receptors on the surface of cancer cells, the cells take medications modified with lactoferrin through endocytosis, increasing drug absorption.²⁰

Tumor hypoxia is often caused by vascular anomalies that hinder the transportation and storage of traditional chemotherapeutic drugs, significantly reducing their effectiveness.^{21,22} Many studies have suggested that certain bacteria, which commonly colonize tumors in hypoxic and immunosuppressed environments, can act as effective delivery systems for targeted tumor therapy. These bacteria include *Salmonella*, *Escherichia*, *Clostridium*, *Bifidobacterium*, *Proteus*, and *Lactobacillus*.^{23,24} Studies have shown that the anaerobic probiotic *Bifidobacterium infantis*, which is naturally present in the gut of infants, can actively target and colonize hypoxic regions of solid tumors following intravenous injection.^{25,26} The concentration of *B. infantis* in these areas can be 1000 times greater than that in normal tissue, making it an ideal candidate for drug delivery owing to its unique targeting ability and biological safety profile.^{27,28}

In this study, celastrol was encapsulated in polyethylene glycolated liposomes with modified lactoferrin attached to their surface to enhance uptake by cancer cells.^{10,29} These liposomes easily attach to bifidobacteria via a carboxymethyl chitosan coating, resulting in the formation of the biomotor Bif@CLC-LP, which precisely colonized the tumor tissue. In the acidic tumor microenvironment, CEL/LF/CMCS-Lipo (CLC-LP) breaks down and releases celastrol liposomes that specifically target the lactoferrin receptor, inducing apoptosis in cancer cells. This strategy showed remarkable anticancer benefits in a lung cancer mouse model.

Materials and Methods

Cells and Animals

A549 and Lewis (LLC) cell lines were purchased from the Chinese Academy of Sciences Cell Bank (Shanghai, China). *Bifidobacterium infantis* (GIM1.207) was purchased from the Microbial Strain Preservation Centre (Guangzhou, China). Male C57BL/6J mice weighing 16–20 g (six weeks old) were purchased from Tengxin Huaifu Laboratory Animal Sales Co., Ltd. (Chongqing, China). The mice were maintained under standard specific standard specific pathogen-free (SPF) conditions at the Animal Experiment Centre of Southwest Medical University. All animal experiments were approved by the ethical and scientific committee of the Animal Care and Treatment Committee of Southwest Medical University (license no. 20230731-001). All animal experimental procedures were performed in accordance with the requirements of the National Research Council's Guide.

Preparation and Characterization of BIF@CEL/LF/CMCS-Lipo Biohybrid

The ethanol injection method was used to prepare celastrol liposomes (Cel-LP). The effects of different formulations on the liposome particle size, PDI, and encapsulation rate were shown in the [Supplementary Material](#). Lactoferrin was then modified on the surface of the celastrol liposomes to form CEL/LF-Lipo (CL-LP), which was subjected to gel electrophoresis, Fourier transform infrared spectroscopy (FT-IR) and nuclear magnetic resonance spectra (NMR) detection. Next, carboxymethyl chitosan was coated to produce CEL/LF/CMCS-Lipo (CLC-LP). The preparation method is described in the [Supplementary Material](#). A suspension containing *B. bifidum* (2.0×10^7 CFU/mL) was incubated with the CLC-LP solution for 3 h at 37 °C, and then the BIF@CEL/LF/CMCS-Lipo (Bif@CLC-LP) biohybrid was obtained by centrifuging the mixture for 3 min at 2500 rpm. The precipitate was washed twice with PBS (pH = 7.4). Transmission electron microscopy (TEM; JEM-1200EX, Japan) and scanning electron microscopy (SEM; SU8020, Japan) were performed to analyze the morphology of the Bif@CLC-LP hybrids. The size and ζ -potential of the celastrol liposomes were determined via dynamic light scattering (DLS, NanoBrook90 plus zeta, Brookhaven, NY).

In vitro Study of the Stability of CEL/LF/CMCS-Lipo

The CEL/LF/CMCS-Lipo (CLC-LP) was immersed in double-distilled water, DMEM, FBS, and PBS at different temperatures and durations. The particle size and ζ -potential were then measured using DLS with a particle size analyzer (NanoBrook 90Plus Zeta, Brookhaven Instruments Corporation, NY, USA).

Drug Release Performance Testing

The optimal absorption peak of celastrol was determined using an ultraviolet (UV) spectrophotometer (UV-5800 PC, Shanghai Metash Instruments Co., Ltd., Shanghai, China). Liposomal nanoparticles were used along with dialysis techniques to evaluate the *in vitro* release properties of celastrol (Cel). A release medium of pH 7.4 or 6.5 PBS (including 20% ethanol) was added to 50 mL centrifuge tubes, along with 2 mL dialysis bags containing Cel, Cel-LP, and CLC-LP. These centrifuge tubes were incubated at 100 rpm and 37 °C on a shaker. At specific time intervals (1, 3, 6, 12, 24, 48, 72, 96, and 120 h), 3 mL of the release medium was extracted from the centrifuge tubes. The same volume of release medium was then added back to the tubes while the original temperature and pH were maintained. The concentration of celastrol in the dissolution medium was measured via a spectrophotometer, and the cumulative release rate of celastrol was calculated.

Cytotoxicity Assay of the Drugs

To determine the harmful effects of different medications (Liposome, Cel, Cel-LP, CL-LP, CLC-LP, and Bif@CLC-LP) on lung cancer cells in a pH-dependent manner, A549 and Lewis cells were seeded in 96-well plates and cocultured with liposome solutions at different concentrations for 24 h. Each well received 20 μ L of thiazolyl blue (MTT) solution (5 mg/mL). The precipitated crystals were diluted in 150 μ L of dimethyl sulfoxide (DMSO) to determine the absorbance using a microplate reader (RedMax, Shanghai Flash Spectrum Biological Technology Co., Ltd., Shanghai, China).

In Vitro Studies of BIF@CEL/LF/CMCS-Lipo Targeting

A549 and Lewis cells were seeded in six-well plates and treated with NR-LP, LF-NR-LP, CL-NR-LP, Bif@CL-NR-LP, or LFR-blocking (the latter was pretreated with a lactoferrin solution at a concentration of 2 mg/mL). After incubation for 3 h, the nuclei were stained with DAPI and subsequently washed three times with PBS (pH = 7.4) before being observed using a fluorescence microscope (OLYMPUS, IX73, Japan).

Cell Migration Assay

A scratch assay was performed to assess the *in vitro* migration of A549 cells. After 5.0×10^5 tumor cells were seeded per well in a six-well plate to confluence, a sterile pipette tip was used to make a scratch. Different drugs (including NS, Cel, Cel-LP, CL-LP, CLC-LP, and Bif@CLC-LP) were administered, and the cells at the site where the scratch was made were washed before being cultured. The migration rate was calculated by analyzing the scratch coverage at 0, 12, and 24 h using a microscope (OLYMPUS, CKX53, Japan).

Cell Apoptosis Assay

First, A549 and Lewis cells were inoculated in six-well plates at a density of 5.0×10^4 cells per well and incubated overnight. The cells were then co-incubated with various drugs (including NS, Cel, Cel-LP, CL-LP, CLC-LP, or Bif@CLC-LP, and the concentration of celastrol was 30 μ g/mL) for 24 h. The cells were harvested, washed twice with PBS (pH = 7.4), and stained with 5 μ L of 647A-Annexin V and 5 μ L of PI dye for 20 min. The apoptosis rate was measured via flow cytometry (DxFLEX, Beckman Coulter). Additionally, apoptosis was evaluated via live-dead cell staining. A549 and Lewis cells were seeded at a density of 1.0×10^5 cells per well in six-well plates and incubated with each drug for 24 h. After being washed twice with PBS (pH 7.4), the cells were stained with calcein-AM (1 μ g/mL) and propidium iodide (PI: 1 μ g/mL) for 30 min. The samples were then observed via fluorescence microscopy (OLYMPUS, IX73, Japan).

Exploring the Antitumor Mechanisms of BIF@CEL/LF/CMCS-Lipo

Lewis cells were treated with drugs (including NS, Cel, Cel-LP, CL-LP, CLC-LP, or Bif@CLC-LP, and the concentration of celastrol was 30 μ g/mL) for 24 h at a density of 5.0×10^4 cells per well in six-well plates. After treatment, the cells were incubated with DCFH-DA dye for 30 min. The cells were washed thrice with PBS (pH = 7.4) and examined using an inverted microscope (OLYMPUS, IX73, Japan). Moreover, JC-1 dye was added to the cells treated with Bif@CLC-LP,

which were then incubated for 30 min. The cells were washed twice with PBS (pH = 7.4), and the mitochondrial membrane potential changes were observed using an OLYMPUS IX73 microscope (Japan).

Bacterial Growth Inhibition Experiment

The semisolid Petri plates were evenly covered with a Bif suspension and incubated overnight. Next, 6 mm drug-sensitive paper tablets were soaked in saline, Cel, Cel-LP, CL-LP, CLC-LP, or Bif@CLC-LP. The tablets were dried, placed in the center of a Petri dish, and then incubated for 24 h at 37 °C. The growth inhibition zone of each tablet was measured.

In Vitro Hemolysis Assay for Celastrol Preparation

The blood compatibility of various formulations was evaluated via an in vitro hemolysis assay. Briefly, 1 mL of 0.2% (v/v) red blood cell suspension was mixed with equal volumes of physiological saline solutions containing Cel, Cel-LP, CL-LP, CLC-LP, and Bif@CLC-LP. Distilled water was used as the positive control, and physiological saline was used as the negative control. Hemoglobin released from erythrocytes was detected at 540 nm using a UV-visible spectrophotometer (UV-5800PC, Shanghai Yuan Instrument Co., Ltd., China). The hemolysis rate was calculated as follows:

$$\text{Hemolysis (\%)} = (\text{OD}_{\text{sample}} - \text{OD}_{\text{negative}}) / (\text{OD}_{\text{positive}} - \text{OD}_{\text{negative}}) 100\%.$$

Anaerobic Targeting Evaluation of BIF@CEL/LF/CMCS-Lipo

The ability of Bif to target hypoxic areas in vitro was assessed. To conduct the assay, the upper chamber of the transwell system was filled with 200 µL of Bif and Bif@CLC-LP suspensions (5×10^7 CFU/mL). In contrast, the lower chamber was made hypoxic by adding 0.4 mL of glucose (0.4 mg/mL), glucose oxidase (0.5 kU), and catalase (0.5 kU). Normal oxygen levels were maintained in the control group. After incubation for 2 h, the number of bacteria that migrated to the lower compartment was determined.

In Vivo Evaluation of the Antitumor Effect of BIF@CEL/LF/CMCS-Lipo

Male C57BL/6J mice were subcutaneously injected with 0.1 mL of Lewis cells suspension (5.0×10^6 cells) in the right leg to construct a tumor model. When the tumor volume reached 50–100 mm³, the mice were randomly divided into five groups as follows (n = 6 per group): NS, Cel, CL-LP, CLC-LP, and Bif@CLC-LP (Cel: 2 mg/kg). Each mouse received an intravenous injection every second day for one week, for a total of three treatments. Tumor size and body weight were measured every two days over two weeks. After two weeks, blood samples were collected via the retroorbital route for blood biochemistry examinations and routine testing. The major organs (including the heart, liver, spleen, lungs, and kidneys) were harvested along with the tumors to conduct various tests and analyses, including H&E staining, TUNEL staining, Sirius red, MPO tests, and immunohistochemical analysis of Ki67.

MicroPET/CT Scanning to Assess Drug Efficacy

Tumor metabolism following medication was evaluated via small animal PET/CT scanning (InveonMM Siemens, Germany). After fasting for 6 h, the mice were injected with 200–250 µCi of ¹⁸F-FDG through the tail vein. These mice were anesthetized via isoflurane inhalation and subjected to whole-body scanning. Two nuclear medicine physicians analyzed the PET/CT scans, identified the region of interest (ROI) manually on the tumor images, and calculated the average uptake value (SUV_{mean}) and the maximum standard uptake value (SUV_{max}).

In vivo Fluorescence Imaging for BIF@CEL/LF/CMCS-Lipo Targeting Studies

To assess the ability of the developed Bif@CLC-LP/ICG biomotor to target tumors, in vivo fluorescence imaging was performed. All samples, including the ICG-labeled Bif@CLC-LP, CLC-LP, and Bif solutions, underwent a dark reaction for 24 h. The nanoparticles were retrieved after being centrifuged and washed three times with deionized water. When the tumor volume reached 100–200 mm³, 0.1 mL of ICG, Bif@CLC-LP/ICG, CLC-LP/ICG, or Bif/ICG was injected

intravenously. Imaging was performed using an IVIS imaging system (FvPro, USA) at 6, 12, 24, and 48 h after injection. The mice were euthanized after 48 h, and the tumors and vital organs were removed for systematic imaging.

Statistical Analysis

All the data are expressed as the means \pm standard deviations (SDs). Statistical analysis was conducted via two-tailed Student's *t* tests or one-way ANOVA in GraphPad Prism. All differences among and between groups were considered statistically significant at $P < 0.05$ (* $P < 0.05$, ** $P < 0.01$, and *** $P < 0.001$).

Results

Preparation and Characterization of BIF@CEL/LF/CMCS-Lipo Biohybrid

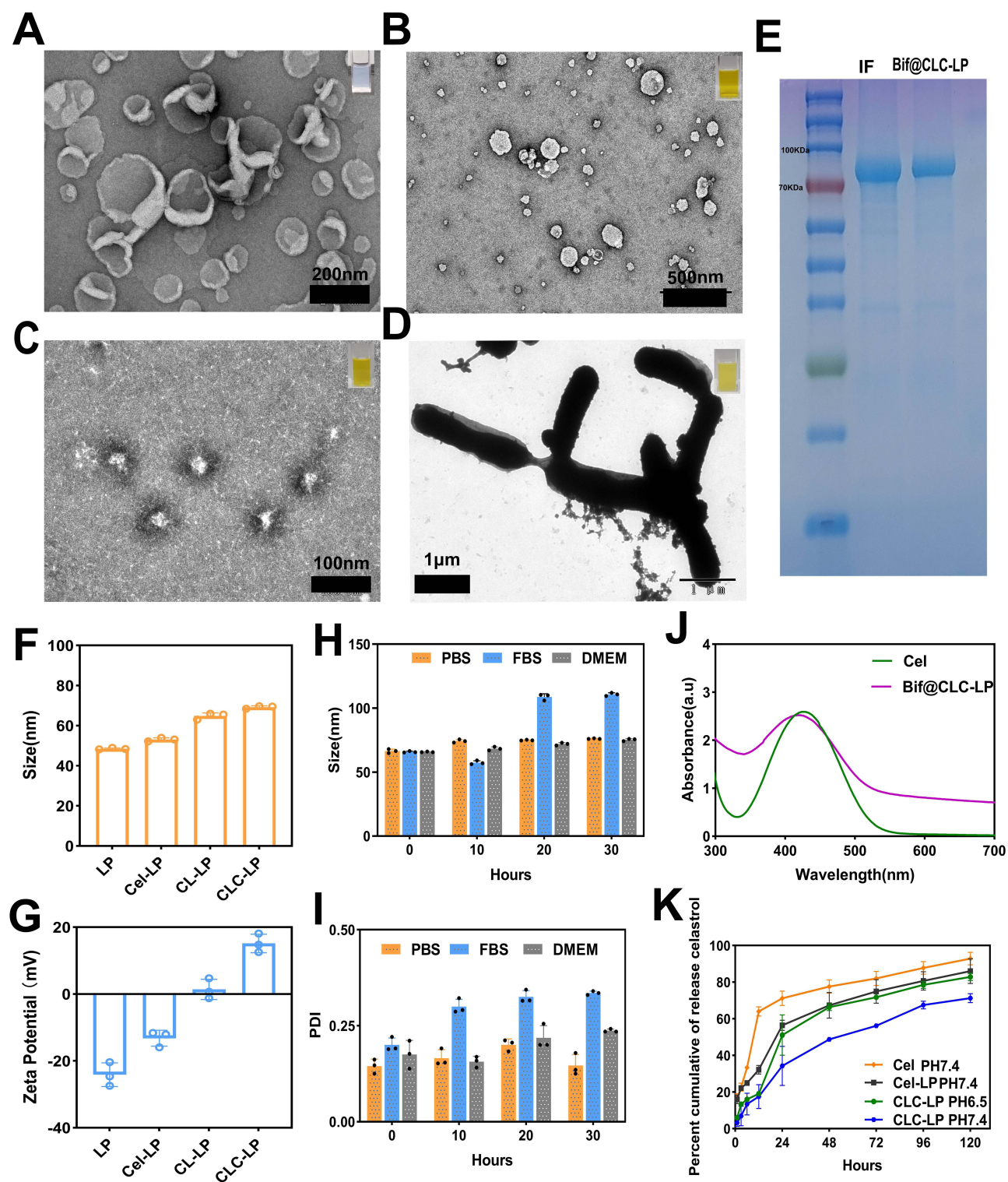
The celastrol-loaded liposomes (Cel-LP) exhibited a solid, spherical shape resembling that of the blank liposomes (LP) (Figure 1A and B). Lactoferrin-modified celastrol (CL-LP) liposomes were coated with an outer layer of carboxymethyl chitosan (CMCS) to form CLC-LP (Figure 1C). The Bif@CLC-LP biohybrid was created by loading CLC-LP onto the surface of *Bifidobacterium bifidum* (Figure 1D and S1, Supplementary Material). Protein electrophoresis experiments revealed that lactoferrin and CL-LP exhibited similar blue streaks in the 75–100 kDa range (Figure 1E). The CL-LP group had a particle size of 64.85 nm (Figure 1F). In contrast, zeta potential measurements revealed a shift from a negative potential in Cel-LP to a positive potential in CL-LP (Figure 1G). FT-IR detection revealed an amide C=O and C-N stretching vibrational peak at 1648 cm^{-1} and 1424 cm^{-1} (Figure S2). NMR showed -CO-NH- formed at 6.13 ppm (Figure S3). These results indicated that lactoferrin was successfully attached to the celastrol liposomes. The liposomes demonstrated good stability in various media, with diameters ranging from about 50–80 nm (Figure 1H and I). Celastrol and Bif@CLC-LP peaked at 424 wavelengths under UV spectrophotometer detection, confirming successful loading of celastrol by Bif@CLC-LP (Figure 1J). Compared with the 34.33% released from the CLC-LP at pH 7.4, 71.22% of the celastrol in the free celastrol group (Cel) was released after 24 h. Additionally, in an environment at pH 6.5, 51.12% of the medication was released from the CLC-LP. These results indicated that the CMCS coating may decompose more easily in an acidic environment, preventing premature or off-target release of the drug (Figure 1K).

In vitro Targeting and Antitumor Effects of BIF@CEL/LF/CMCS-Lipo

The results of the cellular uptake assays revealed that Nile Red-labeled liposomes were taken up by Lewis cells (Figure 2A and B) and A549 cells (Figures S4 and S5). The uptake of lactoferrin-modified liposomes (LF-NR-LP) increased significantly. Pretreatment of Lewis cells with lactoferrin almost completely inhibited the uptake of LF-NR-LP. These findings suggest that lactoferrin competitively binds to lactoferrin receptors on the surface of cancer cells, preventing LF-NR-LP uptake. These results indicated that liposomes modified with lactoferrin can specifically bind to cancer cell surface receptors, increasing the cellular uptake of liposomes. The outer layer of LF-NR-LP coated with CMCS (CL-NR-LP) did not affect its cellular uptake. The Bif@CL-NR-LP group exhibited strong fluorescence intensity, suggesting that the liposomes separated from bacteria and were absorbed by cells. The survival rates of Lewis cells and A549 cells treated with high concentrations of liposomes (1000 $\mu\text{g/mL}$) were 91.22% and 90.98% (Figure 2C and S6). These findings indicate that liposomes are noncytotoxic and can be considered safe and reliable carriers for drugs. The cell viability of CLC-LP decreased from 87.34% to 12.43% in a neutral environment (pH 7.4). Additionally, in a weakly acidic environment (pH 6.5), the cell viability of the CLC-LP decreased from 60.82% to 3.56%, possibly due to the disintegration of the CMCS. Bif@CLC-LP showed similar cytotoxicity (Figure 2D and E). The cytotoxicity results were also confirmed in A549 cells (Figures S7 and S8). Additionally, the 24 h healing rate was 47.27% in the control group, 25.4% in the CLC-LP group, and 23.44% in the Bif@CLC-LP group, confirming that Bif@CLC-LP effectively inhibited the migration of A549 cells (Figure 2F and G).

BIF@CEL/LF/CMCS-Lipo Induces the Apoptosis of Cancer Cells

During the live-dead cell staining experiment, the Lewis cells (Figure 3A and B) and A549 cells (Figure S9) in the Bif@CLC-LP group had a significantly greater number of dead cells than did those in the group treated with free celastrol (Cel). Reactive



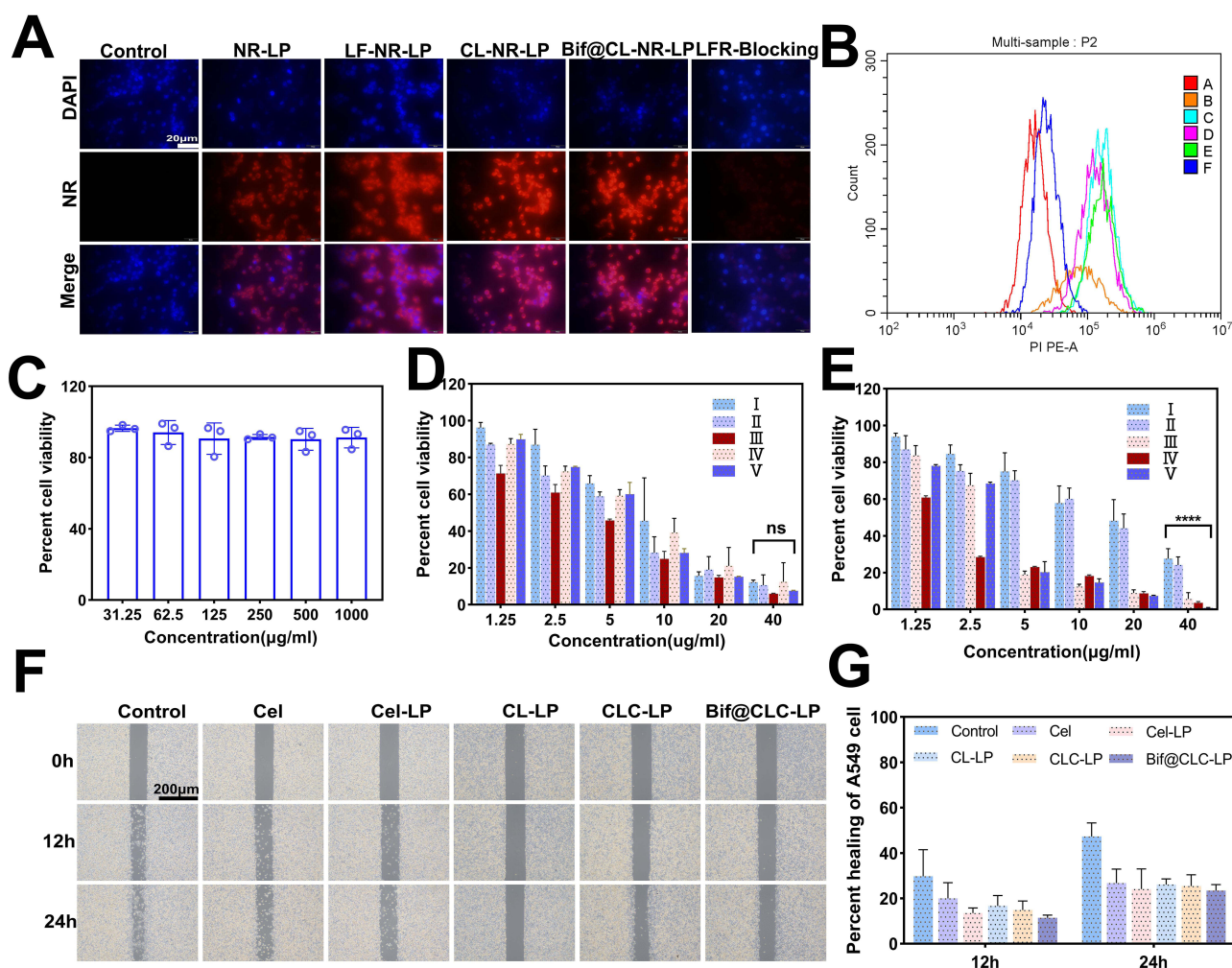


Figure 2 In vitro cell experiments. (A) Fluorescence images of different drugs taken up by Lewis cells; scale bar: 20 μ m. (B) Flow cytometry assay of drugs uptake by Lewis cells. (C) Cytotoxic effects of liposomes on Lewis cells ($n = 3$). (D and E) Cytotoxic effects of different drugs on Lewis cells at pH 7.4 and 6.5. (F) A549 cell scratch experiment; scale bar: 200 μ m. (G) Healing rate of each group; ns: not statistically significant, **** $P < 0.0001$.

Abbreviations: I, Cel; II, Cel-LP; III, CL-LP; IV, CLC-LP; V, Bif@CLC-LP; A, Control; B, NR-LP; C, LF-NR-LP; D, CL-NR-LP; E, Bif@CL-NR-LP; F, LFR-Blocking, the cells were treated with lactoferrin solution in advance.

oxygen species (ROS) were produced intracellularly in Lewis cells via the use of a DCFHDA probe. The distinct green fluorescence, along with the statistical analysis of the average fluorescence intensity, confirmed that, compared with the Cel group, the CL-LP, CLC-LP, and Bif@CLC-LP groups produced high levels of ROS (Figure 3C and F). ROS may be the primary reason for apoptosis in cancer cells. Apoptosis was detected via flow cytometry. The apoptosis rate of Lewis cells treated with Bif@CLC-LP was 93.92%, which was significantly greater than that of the other groups (Figure 3D and G). Similar results were also found in A549 cells (Figure S10 and S11). Additionally, the mitochondrial membrane potential decreased, which likely accelerated apoptosis as a result of mitochondrial dysfunction caused by excess ROS (Figure 3E).

BIF@CEL/LF/CMCS-Lipo Selectively Targets Hypoxic Regions of Tumors

The lack of a distinct inhibitory zone in the drug inhibition trials suggested that the different medications (Cel, Cel-LP, CL-LP, and CLC-LP) did not significantly inhibit bacterial growth (Figure 4A). In the hypoxic zone of the lower chamber, the number of bacteria was considerably greater than that in the normoxic zone of the upper chamber of the transwell system after Bif@CLC-LP was added to the upper chamber for 2 h. This observation indicated that Bif@CLC-LP maintained the anaerobic characteristics of *Bifidobacterium* (Figure 4B and C). Additionally, after Bif@CLC-LP was injected into the mice, the bacteria grew mainly in the kidney, liver, and tumor tissues; the number of bacteria in the tumor tissues was significantly

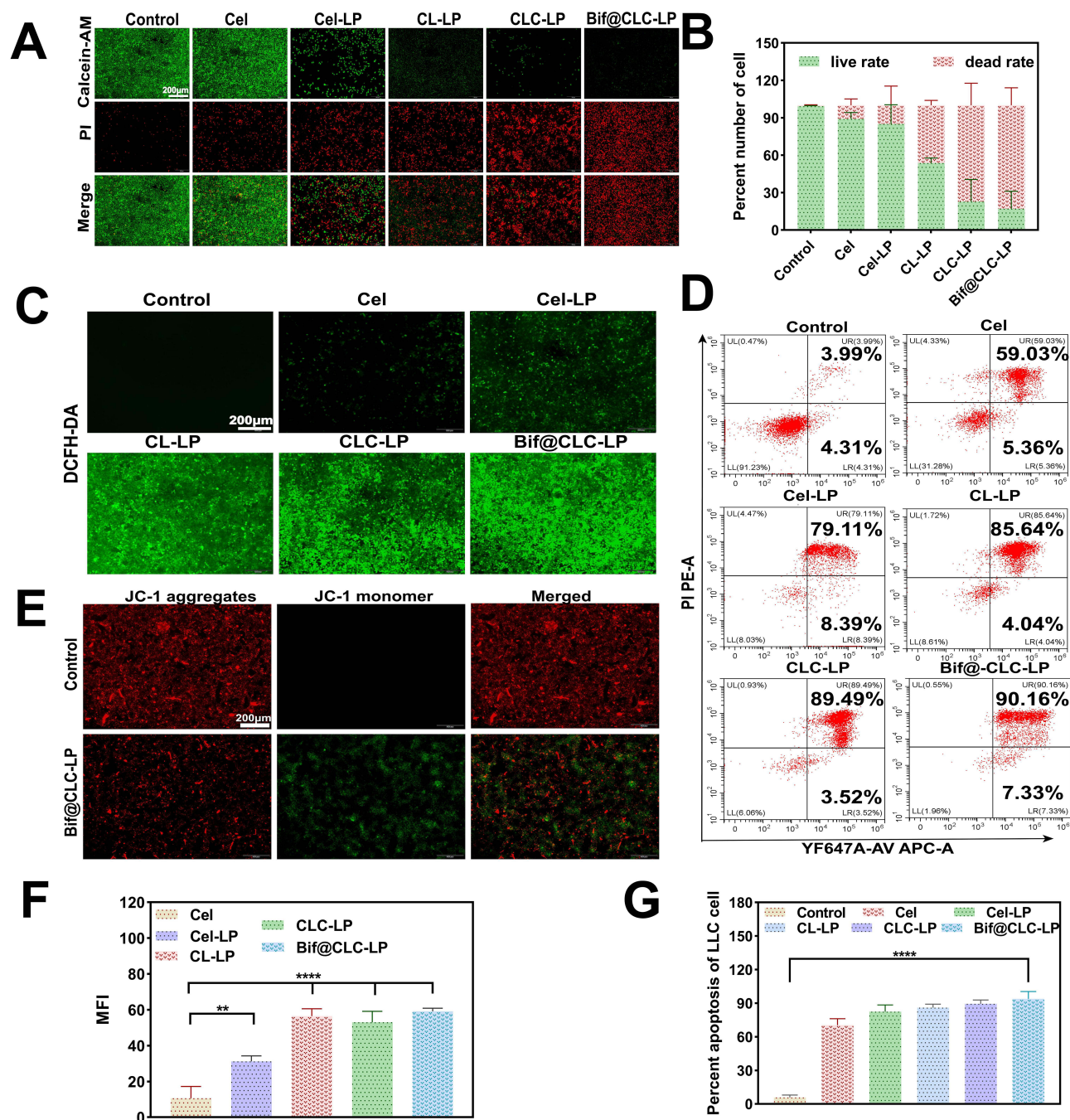


Figure 3 In vitro apoptosis experiments. (A) Live/dead staining of Lewis cells treated with various drugs (NS, Cel, Cel-LP, CL-LP, CLC-LP, Bif@CLC-LP) for 24 h; calcein-AM (green: live cells) and PI (red: dead cells); scale bar: 200 μ m. (B) Live/dead cell rates of each group. (C) Fluorescence images of DCFH-DA-stained tumor cells after treatment with various drugs for 24 h. (D) Flow cytometry analysis was performed on Lewis cells after treatment with different conditions for 24 h. (E) Fluorescence images of Lewis cells treated with Bif@CLC-LP for 24 h and stained with JC-1; scale bar: 200 μ m. (F) Quantitative analysis of DCFH-DA fluorescence in Lewis cells ($n = 3$). (G) Apoptosis rate in each group; ** $P < 0.01$ and **** $P < 0.0001$.

greater than that in the other organs. Greater bacterial colonization was found in tumor tissues one week after injection. These results suggested that Bif@CLC-LP can specifically localize to tumor tissue (Figure 4D).

In vivo Antitumor Effects of BIF@CEL/LF/CMCS-Lipo

Indocyanine green (ICG) was used as a tracer to track the in vivo distribution of Bif@CLC-LP (Figure 5A). Bif-loaded ICG and CLC-LP/ICG showed considerable aggregation in the tumor area at 6 h, reached peak drug accumulation at 24 h, and remained

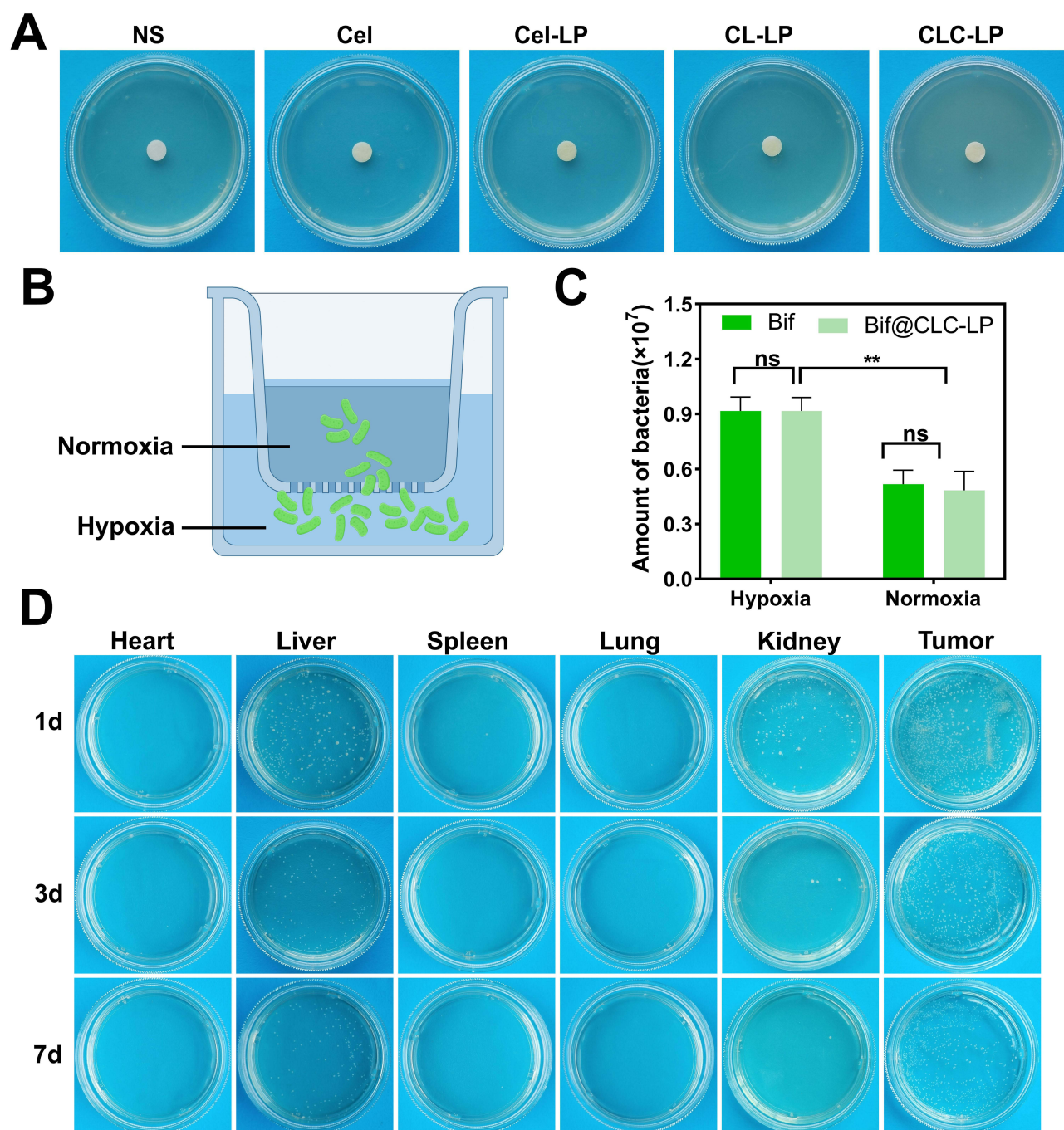


Figure 4 Evaluation of the bioactivity and targeting ability of the biomotor Bif@CEL/LF/CMCS-Lipo. **(A)** The antibacterial effects of various drugs (NS, Cel, Cel-LP, CL-LP, CLC-LP) on Bif. **(B)** A schematic diagram illustrating the hypoxia model in which the transwell system was used to assess the chemotaxis of Bif and Bif@CLC-LP. **(C)** The number of bacteria in the transwell chambers. **(D)** Representative images of bacterial growth in the heart, liver, spleen, lung, kidney, and tumor tissues were captured after Bif@CLC-LP was injected into lung tumor-bearing mice on days 1, 3, and 7; ns: not statistical significance, $**P < 0.01$.

concentrated in the tumor area at 48 h. In contrast, the other groups accumulated only a small amount in the tumor area and were gradually cleared. Among the isolated organ tissues, the Bif@CLC-LP/ICG group presented the greatest tumor accumulation at 5.26×10^{10} (p/s)/($\mu\text{W}/\text{cm}^2$), followed by the liver at 2.18×10^{10} (p/s)/($\mu\text{W}/\text{cm}^2$) and the kidney at 4.15×10^9 (p/s)/($\mu\text{W}/\text{cm}^2$). The other major organs presented significantly lower accumulation levels (Figure 5B). Fluorine-18-labeled deoxyglucose positron emission tomography/computed tomography (18F-FDG PET/CT) imaging was conducted to analyze antitumor metabolism in mice with lung tumors (Figure 5C). The SUVmax of the Bif@CLC-LP group was 1.2 (Figure 5D), and the SUVmean was 0.88

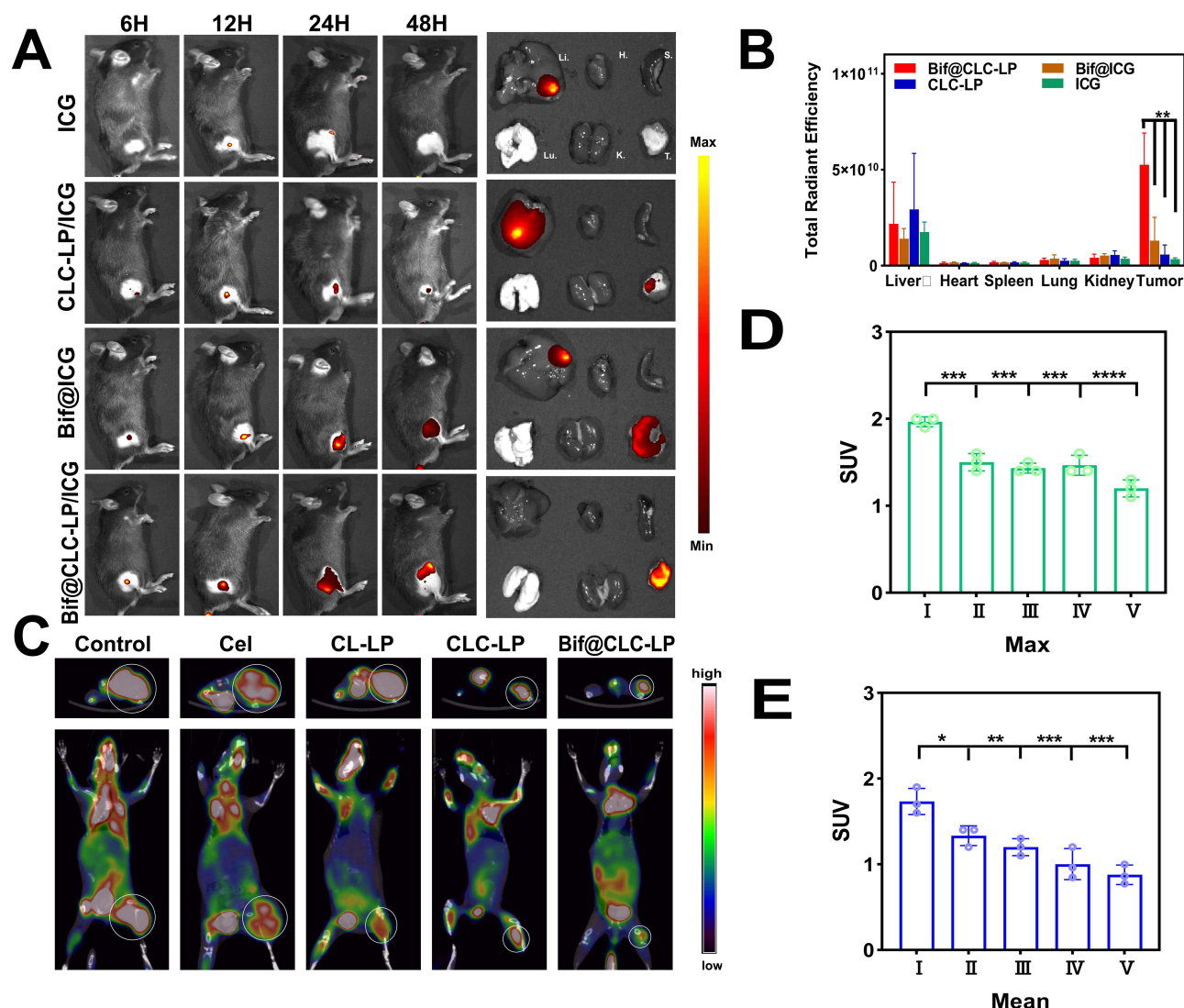


Figure 5 In vivo evaluation of the targeting of Bif@CEL/LF/CMCS-Lipo. (A) Fluorescence images of Lewis lung tumor-bearing mice after intravenous injection of free ICG, CLC-LP/ICG, Bif@ICG, and Bif@CLC-LP/ICG. (B) Total fluorescence counts of isolated organs. (C) Representative images of 18F-FDG PET/CT on day 12 after treatment. Upper layer: cross-sectional images; lower layer: coronal images; the white circles indicate the tumor sites. (D) SUVmax values for each group. (E) SUVmean for each group. * $P < 0.05$, ** $P < 0.01$, *** $P < 0.001$, and **** $P < 0.0001$.

Abbreviations: I, Control; II, Cel; III, CL-LP; IV, CLC-LP; V, Bif@CLC-LP.

(Figure 5E), which was the lowest among all the groups. These findings suggested that tumor glucose metabolism was significantly inhibited by Bif@CLC-LP treatment. These results confirmed that Bif@CLC-LP can effectively target tumor tissues and inhibit tumor growth and metabolism. As shown in the treatment plan outlined in Figure 6A, the mice in the group that received free celastrol were in poor condition. They experienced significant fluctuations in body weight and short survival times, probably due to the toxic effects of the drug. The growth of tumors in the mice treated with Bif@CLC-LP was significantly inhibited (Figure 6B–D). The isolated tumor volume was $44.99 \pm 18.59 \text{ mm}^3$, and the weight was $0.24 \pm 0.04 \text{ g}$, both of which were significantly lower than those in the other groups (Figure 6E and F). Additionally, these mice showed slight changes in body weight and had the longest survival time (Figure 6G and H). H&E and TUNEL staining of the tumor tissue sections revealed a lower tumor cell density, significant apoptotic necrotic areas, and decreased Ki67 expression in the Bif@CLC-LP group than in the other groups (Figure 6I).

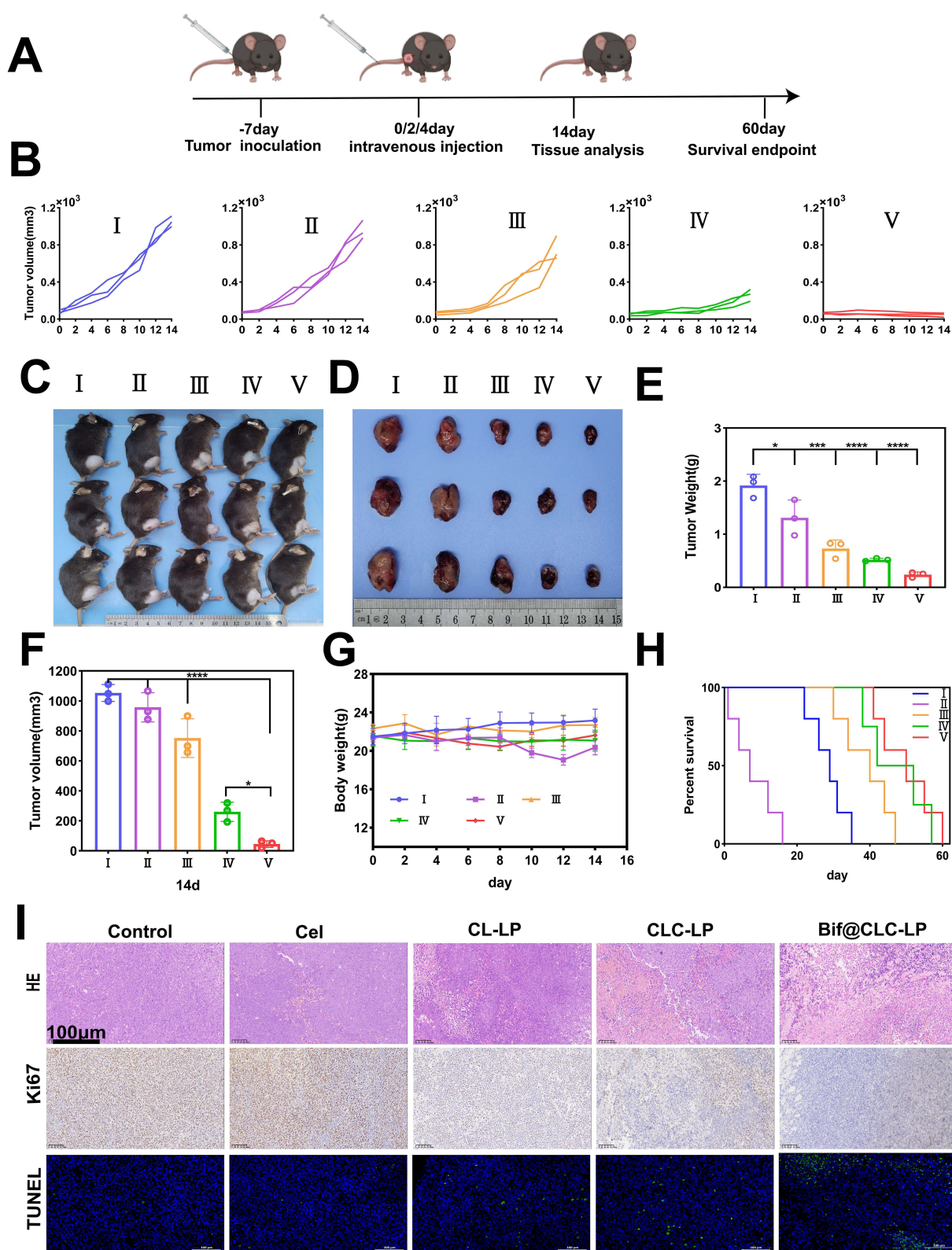


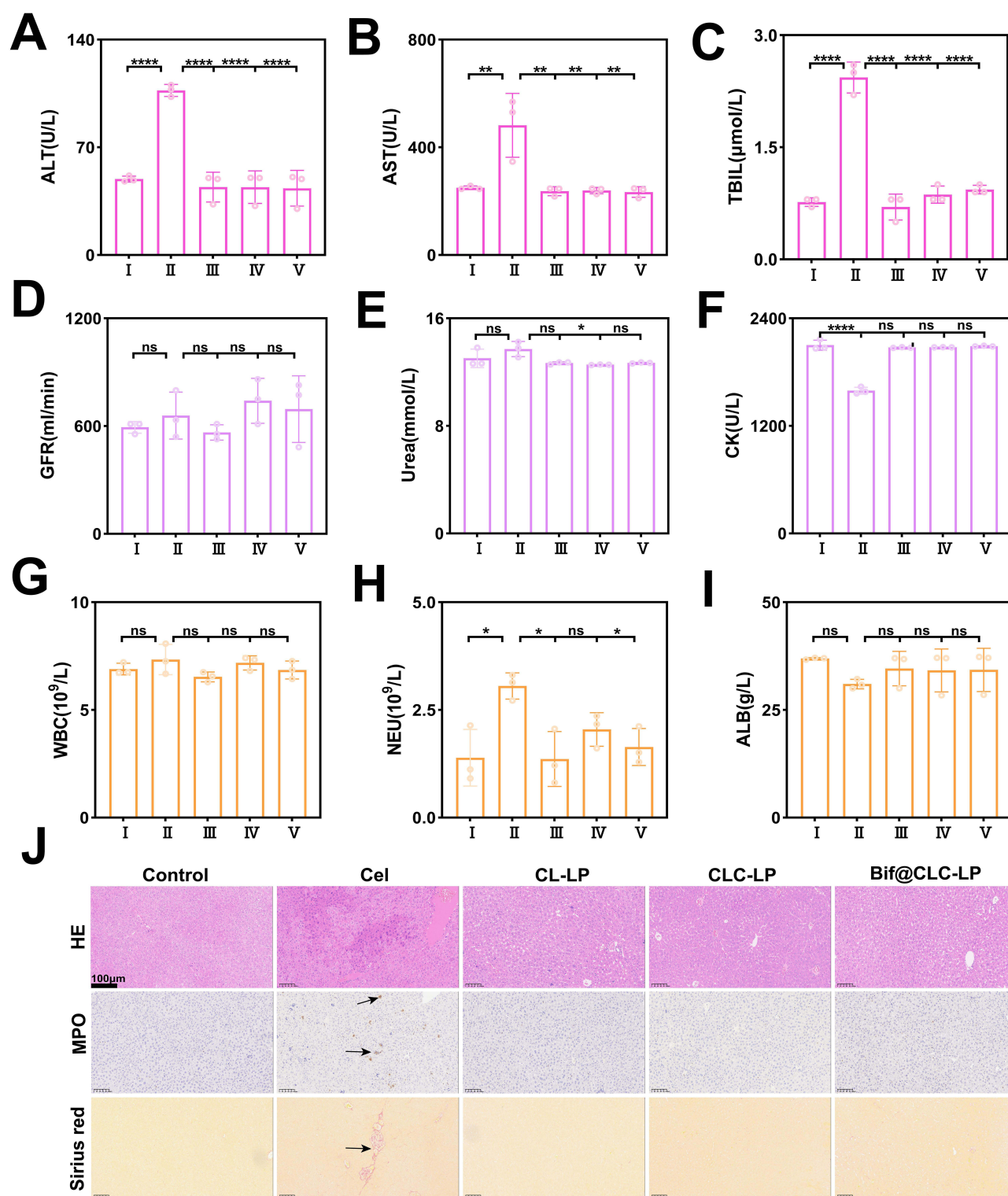
Figure 6 In vivo evaluation of antitumor efficacy of BIF@CEL/LF/CMCS-Lipo. (A) A schematic diagram of the treatment plan. (B) Curve showing growth after each drug treatment was administered. (C) Representative photographs of Lewis lung tumor-bearing mice were taken on day 14 after treatment (n = 3). (D) Representative photographs of isolated tumors (n = 3). (E) Weights of the isolated tumors. (F) Volume of the isolated tumors. (G) Body weight fluctuations during treatment. (H) Survival curves of the mice after the treatments were observed statistically (n = 3). (I) Immunohistochemical staining with H&E, Ki67, and TUNEL. *P < 0.05, **P < 0.01, ***P < 0.001, and ****P < 0.0001. **Abbreviations:** I, Control; II, Cel; III, CL-LP; IV, CLC-LP; V, Bif@CLC-LP.

In vivo Safety of Celastrol Preparation

No hemolytic reactions were detected in the in vitro hemolysis assay for any of the drug groups, indicating that the drugs were compatible with blood and suitable for intravenous injection (Figure S12). Blood analysis revealed that the levels of alanine aminotransferase (ALT), aspartate aminotransferase (AST), total bilirubin (TBIL), white blood cells (WBC), platelets (PLT), and neutrophils (NEU) were significantly greater in the free celastrol group than in the control group, whereas the albumin (ALB), hemoglobin (HGB), and red blood cells (RBC) levels were lower. These results suggest that celastrol may cause liver damage and inflammation in mice. In contrast, the Bif@CLC-LP group did not show abnormalities in these indicators. The levels of GFR, UREA, and CK did not increase substantially (Figure 7A–I and S13–S15). Hepatic necrosis, inflammatory cell infiltration, upregulation of hepatic medullary peroxidase (MPO) expression, and signs of hepatic fibrosis were found in the livers of the mice in the free celastrol group. In contrast, the liver tissue from the Bif@CLC-LP group presented no abnormalities in these indicators (Figure 7J). Additionally, no abnormalities were found in the other major organs, as determined by H&E staining (Figure S16).

Discussion

The development of new chemotherapeutic agents is one way to address resistance to chemotherapy. Celastrol, a triterpenoid with significant anticancer activity, has great potential as a broad-spectrum anticancer drug. However, its toxicity and side effects are causes for concern.³⁰ Nanomedicines provide new solutions for the diagnosis and treatment of cancer.³¹ Bacteria-mediated nano-delivery systems are being studied more extensively for cancer therapy because they are accurate and effective.³² We developed a targeted biohybrid to precisely deliver celastrol in lung cancer treatment. The growth and spread of tumor cells are significantly influenced by hypoxia, acidity, nutrient abundance, and immunosuppression, which characterize the tumor microenvironment (TME).^{33,34} Conventional chemotherapy often has poor efficiency in transporting drugs and effectively targeting tumor tissues. Moreover, vascular anomalies in hypoxic tumor locations also decrease the effectiveness of traditional chemotherapy.³⁵ Using the properties of the TME to develop tumor-targeted medications can increase therapeutic effectiveness and improve the prognosis of cancer patients.³⁶ Additionally, by modifying lactoferrin on the surface of liposomes loaded with celastrol, we increased the uptake of the liposomes by lung cancer cells through receptor-mediated endocytosis.¹⁹ Conversely, cellular uptake decreased significantly when the transferrin receptor was blocked early in the process. Our earlier in vitro findings revealed that tumor cells targeted by lactoferrin can enhance the effectiveness of chemotherapy. Many recent studies have focused on the application of live bacterial therapy in cancer treatment.³⁷ Specific species of bacteria, such as *Escherichia coli*,³⁸ *Salmonella typhimurium*,³⁹ and *Listeria monocytogenes*,⁴⁰ can target tumors. After being injected intravenously, a significant number of bacteria colonize the tumor site, resulting in a 1,000-fold increase in the bacterial concentration in the TME compared with that in other organs.⁴¹ This unique characteristic makes bacteria excellent carriers for medical use. Recent studies have shown that chemoimmunotherapy for cancer via bacteria-loaded drugs that target the oxygen-deprived area of the tumor is effective, indicating that bacteria can be reliable delivery vehicles.^{42,43} Our approach included coating liposomes with positively charged carboxymethyl chitosan, which binds to the negatively charged Bifidobacterium surface and forms BIF@CEL/LF/CMCS-Lipo(Bif@CLC-LP) biohybrids, which is consistent with previous research.^{44–46} Celastrol can be efficiently transported to the tumor site by Bif@CLC-LP. Furthermore, carboxymethyl chitosan prevents celastrol leakage, which occurs when celastrol breaks down in the tumor's acidic environment, thereby decreasing the toxicity of celastrol to the organs. Transwell and bacteriostatic assays revealed that the drug-loaded Bif could still grow and thrive under anaerobic conditions. The anticancer effect of Bif@CLC-LP was confirmed via in vivo fluorescence imaging and microPET/CT, which revealed that Bif@CLC-LP effectively targeted tumor tissues and had strong antitumor effects on lung cancer models. Additionally, Bif@CLC-LP significantly increased the formation of ROS in cancer cells and decreased the mitochondrial membrane potential, as demonstrated by in vitro experiments. These findings may be related to the mechanisms of necrosis and apoptosis in lung cancer cells. Our future studies will focus on determining the efficacy of this delivery system in various tumor models and further investigating the targets of celastrol.



Conclusion

This study used lactoferrin and *B. bifidum* to create a targeted drug delivery system (Bif@CLC-LP) was used to target tumor tissue and control drug release to precisely deliver celastrol. This process leads to the production of high levels of ROS and decreases the mitochondrial membrane potential in cancer cells, ultimately triggering significant antitumor effects while reducing hepatotoxicity. Therefore, applying bifidobacterium-loaded lactoferrin-modified celastrol liposomes may be an effective strategy for precise anticancer therapy.

Data Sharing Statement

All the data needed to support the conclusions are presented in the paper and/or the [Supplementary Materials](#).

Acknowledgments

All the authors are grateful for assistance from Public Center of Experimental Technology, the Affiliated Hospital of Southwest Medical University.

Author Contributions

All the authors made a significant contribution to the work reported, whether in the conception, study design, execution, acquisition of data, analysis and interpretation, or in all these areas; took part in drafting, revising or critically reviewing the article; gave final approval of the version to be published; agreed on the journal to which the article has been submitted; and agreed to be accountable for all aspects of the work.

Funding

This study is supported by the Scientific Research Project of The Affiliated Hospital of Southwest Medical University (Grant Nos. HYX19008, HD20029,2024ZYD0334).

Disclosure

The authors have declared no conflicts of interest in this work.

References

1. Siegel RL, Giaquinto AN, Jemal A. Cancer statistics, 2024. *CA Cancer J Clin*. 2024;74(1):12–49. doi:10.3322/caac.21820
2. Hirsch FR, Scagliotti GV, Mulshine JL, et al. Lung cancer: current therapies and new targeted treatments. *Lancet Lond Engl*. 2017;389(10066):299–311. doi:10.1016/S0140-6736(16)30958-8
3. Meyer ML, Fitzgerald BG, Paz-Ares L, et al. New promises and challenges in the treatment of advanced non-small-cell lung cancer. *Lancet Lond Engl*. 2024;404(10454):803–822. doi:10.1016/S0140-6736(24)01029-8
4. Luo X, Gong X, Su L, et al. Activatable Mitochondria-Targeting Organoarsenic Prodrugs for Bioenergetic Cancer Therapy. *Angew Chem Int Ed Engl*. 2021;60(3):1403–1410. doi:10.1002/anie.202012237
5. Zhou Q, Liu Q, Wang Y, et al. Bridging Smart Nanosystems with Clinically Relevant Models and Advanced Imaging for Precision Drug Delivery. *Adv Sci Weinheim Baden-Wuert Ger*. 2024;11(14):e2308659. doi:10.1002/adv.202308659
6. Wang C, Dai S, Zhao X, et al. Celastrol as an emerging anticancer agent: current status, challenges and therapeutic strategies. *Biomed Pharmacother Biomedecine Pharmacother*. 2023;163:114882. doi:10.1016/j.biopha.2023.114882
7. Lim HY, Ong PS, Wang L, et al. Celastrol in cancer therapy: recent developments, challenges and prospects. *Cancer Lett*. 2021;521:252–267. doi:10.1016/j.canlet.2021.08.030
8. Chen X, Zhao Y, Luo W, et al. Celastrol induces ROS-mediated apoptosis via directly targeting peroxiredoxin-2 in gastric cancer cells. *Theranostics*. 2020;10(22):10290–10308. doi:10.7150/thno.46728
9. Tan Y, Zhu Y, Zhao Y, et al. Mitochondrial alkaline pH-responsive drug release mediated by Celastrol loaded glycolipid-like micelles for cancer therapy. *Biomaterials*. 2018;154:169–181. doi:10.1016/j.biomaterials.2017.07.036
10. Xie X, Zhan C, Wang J, Zeng F, Wu S. An Activatable Nano-Prodrug for Treating Tyrosine-Kinase-Inhibitor-Resistant Non-Small Cell Lung Cancer and for Optoacoustic and Fluorescent Imaging. *Small Weinheim Bergstr Ger*. 2020;16(38):e2003451. doi:10.1002/sml.202003451
11. Zhang X, Xu X, Wang X, et al. Hepatoma-targeting and reactive oxygen species-responsive chitosan-based polymeric micelles for delivery of celastrol. *Carbohydr Polym*. 2023;303:120439. doi:10.1016/j.carbpol.2022.120439
12. Metselaar DS, Meel MH, Benedict B, et al. Celastrol-induced degradation of FANCD2 sensitizes pediatric high-grade gliomas to the DNA-crosslinking agent carboplatin. *EBioMedicine*. 2019;50:81–92. doi:10.1016/j.ebiom.2019.10.062
13. Geng Y, Xiang J, Shao S, Tang J, Shen Y. Mitochondria-targeted polymer-celastrol conjugate with enhanced anticancer efficacy. *J Control Release off J Control Release Soc*. 2022;342:122–133. doi:10.1016/j.jconrel.2022.01.002
14. Mh Z. Liposomes-enabled cancer chemoimmunotherapy. *Biomaterials*. 2025;313:122801. doi:10.1016/j.biomaterials.2024.122801

15. Tenchov R, Bird R, Curtze AE, Zhou Q. Lipid Nanoparticles—From Liposomes to mRNA Vaccine Delivery, a Landscape of Research Diversity and Advancement. *ACS Nano*. 2021;15(11):16982–17015. doi:10.1021/acsnano.1c04996
16. Zhu X, Li S. Nanomaterials in tumor immunotherapy: new strategies and challenges. *mol Cancer*. 2023;22(1):94. doi:10.1186/s12943-023-01797-9
17. Lv Z, Jin L, Cao Y, et al. A nanotheranostic agent based on Nd(3+)-doped YVO(4) with blood-brain-barrier permeability for NIR-II fluorescence imaging/magnetic resonance imaging and boosted sonodynamic therapy of orthotopic glioma. *Light Sci Appl*. 2022;11(1):116. doi:10.1038/s41377-022-00794-9
18. Liang J, Li L, Tian H, et al. Drug Repurposing-Based Brain-Targeting Self-Assembly Nanoplatfrom Using Enhanced Ferroptosis against Glioblastoma. *Small Weinhe Bergstr Ger*. 2023;19(46):e2303073. doi:10.1002/sml.202303073
19. Elzoghby AO, Abdelmoneem MA, Hassanin IA, et al. Lactoferrin, a multi-functional glycoprotein: active therapeutic, drug nanocarrier & targeting ligand. *Biomaterials*. 2020;263:120355. doi:10.1016/j.biomaterials.2020.120355
20. Zhang D, Duque-Jimenez J, Facchinetti F, et al. Transferrin receptor targeting chimeras for membrane protein degradation. *Nature*. 2024;2024:1. doi:10.1038/s41586-024-07947-3
21. Chung AS, Lee J, Ferrara N. Targeting the tumour vasculature: insights from physiological angiogenesis. *Nat Rev Cancer*. 2010;10(7):505–514. doi:10.1038/nrc2868
22. Wang D, Ma W, Zhang Y, et al. A versatile nanoplatfrom carrying cascade Pt nanozymes remodeling tumor microenvironment for amplified sonodynamic/chemo therapy of thyroid cancer. *Biomaterials*. 2025;313:122778. doi:10.1016/j.biomaterials.2024.122778
23. Duong MTQ, Qin Y, You SH, Min JJ. Bacteria-cancer interactions: bacteria-based cancer therapy. *Exp mol Med*. 2019;51(12):1–15. doi:10.1038/s12276-019-0297-0
24. Zhou S, Gravekamp C, Bermudes D, Liu K. Tumour-targeting bacteria engineered to fight cancer. *Nat Rev Cancer*. 2018;18(12):727–743. doi:10.1038/s41568-018-0070-z
25. Zhao J, Huang H, Zhao J, et al. A hybrid bacterium with tumor-associated macrophage polarization for enhanced photothermal-immunotherapy. *ACTA Pharm Sin B*. 2022;12(6):2683–2694. doi:10.1016/j.apsb.2021.10.019
26. Xiao S, Feng C, Mu M, et al. Bacteria-Mediated Bismuth-Based Nanoparticles Activate Toll-Like Receptors for Breast Cancer Photothermal Immunotherapy. *Adv Funct Mater*. 2024;34:2410113. doi:10.1002/adfm.202410113
27. Lu D, Wang L, Wang L, et al. Probiotic Engineering and Targeted Sonoimmuno-Therapy Augmented by STING Agonist. *Adv Sci*. 2022;9(22):2201711. doi:10.1002/advs.202201711
28. Kimura NT, Taniguchi S, Aoki K, Baba T. Selective localization and growth of Bifidobacterium bifidum in mouse tumors following intravenous administration. *Cancer Res*. 1980;40(6):2061–2068.
29. Zhang Z, Yang J, Min Q, et al. Holo-Lactoferrin Modified Liposome for Relieving Tumor Hypoxia and Enhancing Radiochemotherapy of Cancer. *SMALL*. 2019;15(6):1803703. doi:10.1002/sml.201803703
30. Qiu N, Liu Y, Liu Q, et al. Celastrol nanoemulsion induces immunogenicity and downregulates PD-L1 to boost abscopal effect in melanoma therapy. *Biomaterials*. 2021;269:120604. doi:10.1016/j.biomaterials.2020.120604
31. Li J, Zhu L, Kwok HF. Nanotechnology-based approaches overcome lung cancer drug resistance through diagnosis and treatment. *Drug Resist Updat Rev Comment Antimicrob Anticancer Chemother*. 2023;66:100904. doi:10.1016/j.drug.2022.100904
32. Wu L, Bao F, Li L, Yin X, Hua Z. Bacterially mediated drug delivery and therapeutics: strategies and advancements. *Adv DRUG Deliv Rev*. 2022;187:114363. doi:10.1016/j.addr.2022.114363
33. Haynes NM, Chadwick TB, Parker BS. The complexity of immune evasion mechanisms throughout the metastatic cascade. *Nat Immunol*. 2024;25(10):1793–1808. doi:10.1038/s41590-024-01960-4
34. Li B, Wu C, Li Z, et al. Tumor Microenvironment-Activated In Situ Synthesis of Peroxynitrite for Enhanced Chemodynamic Therapy. *ACS Nano*. 2024;18:27042–27054. doi:10.1021/acsnano.4c10012
35. Lu Z, Verginadis I, Kumazoe M, et al. Modified C-type natriuretic peptide normalizes tumor vasculature, reinvigorates antitumor immunity, and improves solid tumor therapies. *Sci Transl Med*. 2024;16(761):eadn0904. doi:10.1126/scitranslmed.adn0904
36. Moon S, Jung M, Go S, et al. Engineered Nanoparticles for Enhanced Antitumoral Synergy Between Macrophages and T Cells in the Tumor Microenvironment. *Adv Mater Deerfield Beach Fla*. 2024;36(44):e2410340. doi:10.1002/adma.202410340
37. Gurbatri CR, Arpaia N, Danino T. Engineering bacteria as interactive cancer therapies. *Science*. 2022;378(6622):858–864. doi:10.1126/science.add9667
38. NCBI. Engineering tumor-colonizing E. coli Nissle 1917 for detection and treatment of colorectal neoplasia - PubMed. <https://pubmed.ncbi.nlm.nih.gov/38245513/>. Accessed September 27, 2024.
39. Nguyen DH, You SH, Ngo HTT, et al. Reprogramming the tumor immune microenvironment using engineered dual-drug loaded Salmonella. *Nat Commun*. 2024;15(1):6680. doi:10.1038/s41467-024-50950-5
40. Selvanesan BC, Chandra D, Quispe-Tintaya W, et al. Listeria delivers tetanus toxoid protein to pancreatic tumors and induces cancer cell death in mice. *Sci Transl Med*. 2022;14(637):eabc1600. doi:10.1126/scitranslmed.abc1600
41. Li J, Dai J, Zhao L, et al. Bioactive Bacteria/MOF Hybrids Can Achieve Targeted Synergistic Chemotherapy and Chemodynamic Therapy against Breast Tumors. *Adv Funct Mater*. 2023;33(42):3254. doi:10.1002/adfm.202303254
42. He T, Wang L, Gou S, et al. Enhanced Immunogenic Cell Death and Antigen Presentation via Engineered Bifidobacterium bifidum to Boost Chemo-immunotherapy. *ACS Nano*. 2023;17(11):9953–9971. doi:10.1021/acsnano.2c11474
43. Li Y, Leng Q, Zhang Y, et al. Anaerobic bacteria mediated “smart missile” targeting tumor hypoxic area enhances the therapeutic outcome of lung cancer. *Chem Eng J*. 2022;438:135566. doi:10.1016/j.cej.2022.135566
44. Fu J, Liu X, Cui Z, et al. Probiotic-based nanoparticles for targeted microbiota modulation and immune restoration in bacterial pneumonia. *Natl Sci Rev*. 2023;10(2):nwac221. doi:10.1093/nsr/nwac221
45. Choi JY, Ramasamy T, Kim SY, et al. PEGylated lipid bilayer-supported mesoporous silica nanoparticle composite for synergistic co-delivery of axitinib and celastrol in multi-targeted cancer therapy. *Acta Biomater*. 2016;39:94–105. doi:10.1016/j.actbio.2016.05.012
46. Zhou M, Liao J, Lai W, et al. A celastrol-based nanodrug with reduced hepatotoxicity for primary and metastatic cancer treatment. *EBioMedicine*. 2023;94:104724. doi:10.1016/j.ebiom.2023.104724

International Journal of Nanomedicine**Dovepress**
Taylor & Francis Group**Publish your work in this journal**

The International Journal of Nanomedicine is an international, peer-reviewed journal focusing on the application of nanotechnology in diagnostics, therapeutics, and drug delivery systems throughout the biomedical field. This journal is indexed on PubMed Central, MedLine, CAS, SciSearch®, Current Contents®/Clinical Medicine, Journal Citation Reports/Science Edition, EMBase, Scopus and the Elsevier Bibliographic databases. The manuscript management system is completely online and includes a very quick and fair peer-review system, which is all easy to use. Visit <http://www.dovepress.com/testimonials.php> to read real quotes from published authors.

Submit your manuscript here: <https://www.dovepress.com/international-journal-of-nanomedicine-journal>